# Gallol-derived ECM-mimetic adhesive bioinks exhibiting temporal shear-thinning and stabilization behavior☆

**Mikyung Shin**[a,b], **Jonathan H. Galarraga**[b], **Mi Y. Kwon**[b], **Haeshin Lee**[a], **Jason A. Burdick**[b,*]

[a]Department of Chemistry, Korea Advanced Institute of Science and Technology (KAIST), 291 University Road, Yuseong-gu, Daejeon 34141, South Korea

[b]Department of Bioengineering, University of Pennsylvania, 210 South 33rd Street, Philadelphia, PA 19104, USA

## Abstract

3D bioprinting is an attractive technique to fabricate well-organized, cell-laden constructs for tissue repair and disease modeling. Although numerous hydrogel bioinks have been developed, materials are still needed that mimic the cellular microenvironment, have the appropriate viscosity and stabilization for printing, and are cytocompatible. Here, we present a unique gallol-modified extracellular matrix (ECM) hydrogel ink that is inspired by rapid fruit browning phenomena. The gallol-modification of ECM components (e.g., hyaluronic acid, gelatin) allowed (i) immediate gelation and shear-thinning properties by dynamic hydrogen bonds on short time-scales and (ii) further auto-oxidation and covalent crosslinking for stabilization on longer time-scales. The gallol ECM hydrogel ink was printable using an extrusion-based 3D printer by exploiting temporal shear-thinning properties, and further showed cytocompatibility (~95% viability) and on-tissue printability due to adhesiveness of gallol moieties. Printed cell-laden filaments degraded and swelled with culture over 6 days, corresponding to increases in cell density and spreading. Ultimately, this strategy is useful for designing hydrogel inks with tunable properties for 3D bioprinting.

**Statement of Significance**—3D bioprinting is a promising technique for the fabrication of cell-laden constructs for applications as *in vitro* models or for therapeutic applications. Despite the previous development of numerous hydrogel bioinks, there still remain challenging considerations in the design of bioinks. In this study, we present a unique cytocompatible hydrogel ink with gallol modification that is inspired by rapid fruit browning phenomena. The gallol hydrogel ink has three important properties: i) it shows immediate gelation by dynamic, reversible bonds for shear-thinning extrusion, ii) it allows spontaneous stabilization by subsequent covalent crosslinking after printing, and iii) it is printable on tissues by adhesive properties of gallol moieties. As such, this work presents a new approach in the design of hydrogel inks.

## 1. Introduction

Three-dimensional (3D) biofabrication is an emerging research field for tissue engineering [1-3], pharmaceutical screening [4,5] and drug manufacturing [6,7]. Among 3D fabrication techniques, such as nano/micro fluidics [8,9], photolithography [10], electrospinning [11,12], and bioprinting [13,14], extrusion-based 3D bioprinting has been widely used since it is a facile, rapid manufacturing process and viable cells can often be encapsulated during the printing process [15]. Recently, a variety of bioinks have been developed for the extrusion-based printing of cell-laden constructs [15]. These are mostly fabricated from hydrogels due to their high water content and properties that mimic aspects of the extracellular matrix (ECM) [16]. To date, hydrogel inks typically consist of natural (e.g., gelatin (GEL), hyaluronic acid (HA), alginate, chitosan, collagen, and decellularized extracellular matrices) [14,17-23] or synthetic (e.g., poly(ethylene glycol), pluronics) [24-26] polymers, which often include functional modification to support printability and shape fidelity of printed constructs.

There remain challenges to designing hydrogel inks for extrusion-based 3D printing. First, the inks should have low viscosity within the nozzle during extrusion, which is often facilitated through shear-thinning properties. A recent study demonstrated a relationship between rheological, thixotropic properties of hydrogels and 3D printability [27]. Second, the inks should be temporally aged for stabilization to improve shape fidelity of the printed constructs. Additionally, these processes should be cytocompatible, including limiting shear forces on cells and maintaining nontoxic crosslinking processes. Thus, to meet these criteria, it is important to control the crosslinking, as the crosslink type (e.g., covalent, non-covalent) and gelation kinetics control injectability during extrusion, as well as dictate the hydrogel physicochemical properties after printing.

One of the most commonly explored systems is covalent crosslinking of modified polymers via photo-induced radical polymerization with ultraviolet (UV) irradiation, such as with gelatinmethacrylamide (GEL-MA) bioinks [14,23]. However, the printing of GEL-MA-based bioinks requires a gelatin concentration higher than 7–15% [14], resulting in high stiffness of the constructs and decreased cellular activity. In addition to covalent crosslinking, non-covalent, ionic bonds (e.g., alginate-$Ca^{2+}$ interactions) are widely used for gelation with a coaxial nozzle apparatus or spraying system of the crosslinker [28], but the dissociation of such ionic bonds often occurs within several hours and can limit stability [29]. Recent approaches have focused on using dynamic, reversible bonds for shear-thinning and irreversible covalent bonds for stable network formation [17,30,31], such as with host-guest interactions (e.g., cyclodextrin-admantane complexes) [30] or reversible covalent bonds (e.g., aldehyde-hydrazide) [31].

Here, we developed a hydrogel ink based on ECM components (e.g., HA, GEL) modified with gallol moieties that permit control over crosslinking for 3D bioprinting. Gallol

moieties, aromatic rings with three hydroxyl groups, are anti-oxidant chemicals found in a variety of plants, fruits, vegetables and nuts [32]. In food science, gallols have been known as polyphenols associated with rapid fruit browning phenomena [33] and astringency of fruit peels [34,35]. Along with mussel-inspired catechol chemistry (e.g., aromatic rings with two hydroxyl groups), gallol-modified polymers are being developed as tissue adhesives [36,37] and protein-encapsulated depots [38,39]. Tannic acid, which presents numerous gallol groups, has also been incorporated into biomaterials and exhibits high affinity to biomacromolecules, DNA [40] and proteins [39].

In our design, we prepared gallol-modified HA (e.g., HA-Ga) and gelatin-gallol (e.g., GEL-Ga) that (i) gels when mixed through non-covalent hydrogen bonding between gallols and protein backbones and (ii) slowly covalently crosslinks through a spontaneous oxidation process. Our previous study demonstrated shear-thinning properties of gallol-abundant hydrogels [38], which presented high concentrations of small gallol chemicals that could potentially be toxic to cells [41]. In contrast, the use of gallol-modified ECM components in this study enabled both stable crosslinking between gallols and polypeptides, despite only small molar amounts of gallols incorporated, and high viability of encapsulated cells. Towards the development of a unique hydrogel ink for biomedical applications, this material system was explored for 3D extrusion-based printing and for direct printing onto tissues to exploit its adhesive properties.

## 2.    Materials and methods

### 2.1.    Materials

Sodium hyaluronate (HA; Molecular weight (MW) 151–300 kDa) was purchased from Lifecore Biomedical (U.S.A.). Gelatin from porcine skin (Type A, Bloom number of ~300 g), N-(3-Dime thylaminopropyl)-N′-ethylcarbodiimide hydrochloride (EDC), N-hydroxysuccinimide (NHS), 5-hydroxydopamine hydrochloride (MW 205.64), Folin and Ciocalteu's phenol reagent (with a concentration of 2 M), urea (with a stock concentration of 8 M), cardio-green, rhodamine B, and bovine serum albumin (BSA) were obtained from Sigma-Aldrich (U.S.A.). In addition, Dulbecco's Phosphate-Buffered Saline (DPBS, pH 7.4) and Dulbecco's Modified Eagle's medium (DMEM) were purchased from Gibco Life Technologies (U.K.).

### 2.2.    Synthesis and characterization of gallol-modified hyaluronic acid (HA-Ga) and gelatin (GEL-Ga)

To prepare both gallol-modified polymers, EDC/NHS coupling reactions were performed at pH 4.5–5.0. For synthesis of HA-Ga, HA (50 mg) was dissolved in Milli-Q water (9 mL). EDC (126 mg, 5 molar equivalents to the carboxyl group of HA) was added to the HA solution and incubated under stirring for 10 min. Subsequently, NHS (152 mg, 10 molar equivalents to the carboxyl group of HA) was added to the HA/EDC solution. After stirring for 20 min, 5-hydroxydopamine solution (108 mg, dissolved in 1 mL of Milli-Q water, 4 molar equivalents to the carboxyl group of HA) was added drop-wise into the HA/EDC/NHS mixture and reacted for 6 h. The solution was then dialyzed in 2-(N-morpholino)ethanesulfonic acid (MES) buffer (17 mM, pH 4.5–5.0) containing 150 mM

NaCl for 2 days and distilled water alone for 4 h to remove unreacted 5-hydroxydopamine, EDC, and NHS, using a regenerated cellulose dialysis membrane (6000 – 8000 Da). The final product was obtained after lyophilization.

For preparation of GEL-Ga, gelatin (100 mg) was dissolved in Milli-Q water (10 mL) for 1 h at 40 °C. Similar to the synthesis of HA-Ga, EDC (115 mg) was added to the gelatin solution. After activation for 10 min, NHS (138 mg) was added to the gelatin/EDC solution. After 20 min, 5-hydroxydopamine (50 mg) was slowly added to the gelatin/EDC/NHS solution, and the reaction was carried out for 6 h at 40 °C. Thereafter, unreacted 5-hydroxydopamine, EDC and NHS were removed by dialysis (6000–8000 Da) in 150 mM NaCl (pH 4.5–5.0) at 50 °C for 5 days and distilled water for 4 h. The final product was obtained after lyophilization.

To evaluate the degree of gallol conjugation, Folin and Ciocalteu's phenol assay [42] and proton nuclear magnetic resonance ($^1$H NMR) spectroscopy analysis were performed. For the Folin and Ciocalteu's phenol assay, HA, HA-Ga, gelatin, or GEL-Ga was dissolved in Milli-Q water at a concentration of 5 mg mL$^{-1}$. Each solution (20 μL) was added into a 96-well clear UV-transparent microplate (Corning, U.S.A.). Folin and Ciocalteu's phenol reagent (2 M) was diluted ten-fold with Milli-Q water to a final concentration of 0.2 M and the diluted reagent (100 μL) was added to each sample well. Afterwards, 80 μL of 1 M NaOH was added to the well, and the samples were incubated for 2 h at room temperature. After the incubation, absorbance at 750 nm was measured using a microplate reader (Tecan Infinite M200, Switzerland). The gallol standard curve ($A_{750}$) was established by measuring the absorbances of 5-hydroxydopamine solutions ranging in concentrations from 0.068 to 0.54 mg mL$^{-1}$. In addition, $^1$H NMR spectra (DMX 360, Bruker, Billerica, MA, U.S.A.) were obtained using HA-Ga (10 mg) dissolved in 600 μL of deuterium oxide (D$_2$O; Sigma-Aldrich) and GEL-Ga (18 mg) in D$_2$O (1 mL).

### 2.3. Preparation and mechanical testing of ECM-mimetic gallol hydrogels

ECM-mimetic gallol hydrogels were prepared by simply mixing HA-Ga solution (25 mg mL$^{-1}$, dissolved in DPBS) and GEL-Ga (100 or 200 mg mL$^{-1}$, dissolved in DPBS) at a final mass ratio of 1:0, 1:1, or 1:2 (HA-Ga:GEL-Ga). In addition, mixtures at low concentrations of HA-Ga (0 or 20 mg mL$^{-1}$) and GEL-Ga (200 mg mL$^{-1}$) were prepared. For spontaneous gelation, the mixture was vigorously vortexed for approximately 2 min. Furthermore, for aged hydrogels, gallol hydrogels with a ratio of 1:2 were incubated for 24 h at room temperature.

Initial gelation of HA-Ga and GEL-Ga and rheological properties of hydrogels after aging were examined using an AR2000 stress controlled rheometer (TA Instruments, U.S.A.) with a 20 mm diameter cone and plate geometry and gap size of 26 μm. The rheological properties were measured at 37 °C under frequency sweeps ranging from 0.01 to 10 Hz (0.5% strain). As controls, other combinations, such as HA/gelatin, HA-Ga/gelatin, and HA/GEL-Ga, were prepared in the same manner as the gallol hydrogels (e.g., final mass ratio of 1:2, HA-Ga:GEL-Ga). To demonstrate shear-thinning behavior, the shear viscosity of the gallol hydrogels was measured in continuous flow with shear rates from 0.01 to 100 s$^{-1}$. Moreover, the self-recovery properties of hydrogels were evaluated under cycling of

intermittent strains of 0.5 and 1000% for hydrogels early after mixing and 2000% for hydrogels aged for 24 h. Each step was continued for 5 min at 1 Hz frequency.

Gallol hydrogels (50 μL, at a final mass ratio of 1:2, HA-Ga:GEL-Ga) with a cylindrical shape were prepared in a syringe with an inner diameter of 4.76 mm. Compression testing was performed on a Dynamic Mechanical Analyzer (TA Instruments, Q800, U.S. A.). The hydrogels (initial hydrogels after mixing of 2 min or aged hydrogels after 24 h) were retained within a fluid cup under a 0.01 N pre-load and were subsequently compressed until failure at a rate of 0.5 N min$^{-1}$. Young's moduli were calculated as the slope in the linear range between 10 and 25% strain.

### 2.4. In vitro erosion test of gallol hydrogels after aging

For *in vitro* erosion analysis of the gallol hydrogels, hydrogels (50 μL, at a final mass ratio of 1:2, HA-Ga:GEL-Ga) with a cylindrical shape were prepared in a syringe similar to those above. The initial mass of hydrogels was measured and the hydrogels were incubated in DPBS (pH 7.4, 2 mL) supplemented with 10% BSA at 37 °C. Hydrogel masses were then measured after 1, 2, 4, 6, 8, 10, 12, and 14 days, and the relative mass change (× fold) was calculated as the remaining hydrogel mass divided by the initial mass.

### 2.5. Gelation mechanism studies for gallol hydrogels

To better understand the gelation and crosslinking mechanisms involved in fabricating gallol hydrogels, oscillatory rheology, attenuated total reflection infrared (ATR-IR) spectroscopy, and ultraviolet/visible (UV/vis) spectroscopy were used. For rheological testing, three different types of gallol hydrogels were fabricated, including HA-Ga and GEL-Ga dissolved in Milli Q water, DPBS alone, and DPBS containing urea (1 M). The rheological properties of these gels were monitored at 0.5% strain (37 °C) under frequency sweeps ranging from 0.01 to 10 Hz. In addition, for ATR-IR analysis, HA-Ga (2 wt%, 200 μL), GEL-Ga (2 wt%, 200 μL), and the mixture of HA-Ga and GEL-Ga with a final mass ratio of 1:1 were lyophilized for one day. The IR spectra of all samples were measured using a Nicolet 6700 FT-IR spectrometer equipped with an ATR accessory (Thermo Fisher Sci., U.S.A.). For UV/vis absorption tests, HA-Ga (1.25 mg mL$^{-1}$), GEL-Ga (1.25 mg mL$^{-1}$), and the mixture (each with a final concentration of 1.25 mg mL$^{-1}$) were prepared in Milli Q water or DPBS. In a 96-well microplate, HA-Ga, GEL-Ga, and the HA-Ga/GEL-Ga mixture with a final mass ratio of 1:1 were set at the same volume of 200 μL, and absorbances at 420 nm (A$_{420}$) were measured using a microplate reader (Tecan Infinite M200, Switzerland) at pre-determined time intervals of 0.5, 1, 2, 4, 8, and 24 h.

### 2.6. 3D printing for line and lattice construction

For 3D printing, we immediately loaded 60–80 μL of the gallol hydrogels with a final mass ratio of 1:2 (e.g., HA-Ga:GEL-Ga) and total polymer concentration of 6 wt% into syringes. To remove air bubbles, gallol hydrogel-loaded syringes were centrifuged at 1000×$g$ for 3 min. To visualize printed filaments, rhodamine B (3 μL, 20 mg mL$^{-1}$) was added to the HA-Ga solution before adding GEL-Ga. Printed filaments were fabricated via a stepper motor-driven piston-based nozzle and a modified extruder on a commercial 3D Fused Deposition Modeling printer (Revolution XL, Quintessential Universal Building Device). 3D printing

was performed as a function of time after mixing, with printing times of 0.5, 1, and 2 h. Two-layer lattices with dimensions of 0.8cm × 0.8 cm for each layer were generated by standard software to generate G-code (Slic3r) and to control hardware (Repetier). Cover glass (2.2 cm× 2.2 cm), sliced pieces of porcine heart (myocardium), and sliced pieces of porcine lung tissue were used as substrates for printing. The printability of the ink with a total concentration of 4 wt% at an equal mass ratio was also investigated. Finally, constructed lattices and filaments (in air or in DPBS with 10% BSA) were observed using an epifluorescence microscope (Olympus BX51, Japan).

## 2.7. Cell encapsulation and cell viability after printing

For cell studies, all materials were used after sterilization by irradiation for 30 min with a germicidal lamp. Prior to printing, NIH 3T3 fibroblasts were cultured in DMEM supplemented with 10% fetal bovine serum and 1% penicillin/streptomycin. After the cells were washed using sterilized DPBS containing 0.5% penicillin/streptomycin and trypsinized (0.05%), the cells were resuspended in HA-Ga solution at a final concentration of $5 \times 10^6$ cells mL$^{-1}$. Subsequently, GEL-Ga solution was added into the cell-laden HA-Ga solution, with gentle mixing prior to printing.

To investigate cellular viability after printing, a Live/Dead assay kit (Thermo Fisher Sci., U.S.A.) was utilized at culture times of 0, 1, 2, 3, 4, and 6 days after printing. Cells encapsulated in printed constructs were stained with calcein AM (2 μM)/ethidium homodimer (4 μM) working solution (200 μL) for 1 h and observed using an epifluorescence microscope (Olympus BX51, Japan). In addition, the number of live or dead cells was analyzed using ImageJ software, and cellular viability (%) was calculated as follows.

$$\text{Cell viability} \, (\%) \, \text{per field} \, (\times 4 \, \text{magnitude}) = \frac{\text{Live cells}}{\text{Total live and dead cells}} \times 100$$

Relative cell density (× fold) of the live cells was also calculated by normalizing to the cell number observed at one-day of culture. Furthermore, cellular morphology was observed at 20× using an epifluorescence microscope. The projection area (μm$^2$) of cells was analyzed using ImageJ software. To analyze single cell shapes, cells were fixed with 10% formalin for 30 min and stained with rhodamine-phalloidin for 1 h (diluted 1:100, Thermo Fisher Sci., U.S.A.) to visualize F-actin and Hoechst stain for 40 min (5 μgmL$^{-1}$, Thermo Fisher Sci., U.S.A.) to visualize nuclei. Cell morphology was visualized with high magnification (×63) using confocal microscopy (Leica TCS SP5, Germany).

## 2.8. Adhesive strength measurement of gallol hydrogels alone and as inks

To measure the adhesive strength of gallol hydrogels (at 1:2 mass ratio and 6 wt%), polydimethylsiloxane (PDMS) substrates were prepared (1 cm× 5 cm, thickness of 5 mm). One drop of gallol hydrogel macromer solution or non-gallol solution (HA/GEL mixture at a mass ratio of 1:2) was applied onto a substrate area of 1 cm× 1 cm with overlapping pieces of PDMS. After overnight incubation, uniaxial tensile testing was performed (Instron 5848, U.S.A., 10 N load cell), where stresses were exerted on hydrogels via the extension of

PDMS substrates at a rate of 5 mm min$^{-1}$ until failure of the adhesive-adhered interface was observed. To evaluate the tissue adhesive strength of printed gallol inks (at 1:2 mass ratio and 6 wt%), two-layer lattices (0.8 cm× 0.8 cm, 9 lines for each layer) were printed onto porcine myocardium in the same manner as above (Section 2.6) and a block of myocardium tissue (0.8cm × 0.8cm × 3 cm) was placed on top and incubated for 4 h. Tensile testing was performed as described above on overlapping tissue substrates with a 5 N load cell and an extension rate of 5 mm min$^{-1}$. As control groups, non-gallol solutions and PBS were used at the same volume (~25 μL) as printed lattices to overlap tissue substrates. For all of the samples evaluated via tensile testing, the load (N) and the extension (mm) were recorded (Instron Blue- hill software) and the final adhesive strength (kPa) was calculated as the maximum load (kN) divided by the sample cross-sectional area (m$^2$).

### 2.9. Statistical analysis

All statistical analysis was performed using Graphpad Prism 7 software. All data (mean ± s.d.) are in triplicate or more. Comparisons between two groups were performed by un-paired *t*-tests, and data for multiple groups were compared using one-way analysis of variance (ANOVA), post-hoc testing with p value < 0.05 indicating statistical significance.

## 3. Results

### 3.1. Formation of gallol ECM hydrogels and their rheological characterization

The general approach for the formation of gallol ECM hydrogels involves the mixing of gallol-modified ECM components (e.g., HA and GEL) to form hydrogels that have temporal properties that vary from short-term (where hydrogen bonding drives association) to long-term (where oxidative covalent crosslinking drives association) (Fig. 1). For preparation of the gallol ECM hydrogels, HA and GEL were modified with 5-hydroxydopamine hydrochloride via EDC/NHS coupling reaction [38].

The degrees of gallol conjugation to each polymer, HA-Ga or GEL-Ga (Fig. S1A), were determined by Folin and Ciocalteu's phenol assay (Fig. S1B) and $^1$H NMR spectroscopy (Fig. S1C and D). The Folin and Ciocalteu's phenol assay is a standardized colorimetric assay for measuring the total amount of polyphenols based on their antioxidant behavior in food and plant sciences [42]. In this colorimetric assay, phenolic compounds are oxidized in alkaline condition, and the phosphomolybdic/phosphotungstic acid complex is simultaneously reduced with a blue color change (750 nm). The absorbance (750 nm) of the HA-Ga (e.g., 100 μg) was 0.18 ± 0.02 (Fig. S1B), indicating conjugation of 11.0 ± 2.5%, whereas no colorimetric changes were observed in unmodified HA. In the $^1$H NMR spectrum of HA-Ga, proton peaks appeared at 6.3 ppm (a) for the aromatic protons of gallol groups (C2 and C6) and 2.8 ppm (b) for the four ethyl protons tethered to C5, indicating a conjugation of 14% when comparing the integration value of the ethyl protons (b) to that of the methyl protons (1.9 ppm) on the HA backbone (Fig. S1C). The unmodified GEL showed an intrinsic absorbance (750 nm) of 0.10 ± 0.01 due to phenol groups in the side chain of tyrosine [43], whereas the absorbance of GEL-Ga was 0.21 ± 0.01 (Fig. S1B). On the basis of the carboxyl groups in the side chains of aspartic acid and glutamic acid (e.g., 0.12 μmol of −COOH per 100 μg of GEL) [44], the conjugation in GEL-Ga was determined to be 15.0

± 2.9%. Furthermore, in the ^{1}H NMR spectrum, the peak at 2.8 ppm (c) for the four ethyl protons tethered to C5 of gallol groups appeared (Fig. S1D). As a standard signal in the polypeptide backbone of GEL, the peak for the valine (Val), leucine (Leu), and isoleucine (Ile) side chains appeared at 1.3 ppm (18 protons) [44], which was used to calculate a conjugation of 13.9%, similar to the results of the colorimetric assay. Although the gallols have a high affinity to proteins [38,39], the GEL-Ga with a conjugation of only ~13–15% retained sol status at early times and did not show self-crosslinking in solution at 37 °C (e.g., a concentration of 4wt%) (Fig. S2).

Spontaneous gelation (storage modulus (G′) greater than the loss modulus (G″)) occurred with the mixture of HA-Ga and GEL-Ga, referred to as gallol ECM, within 2 min under physiological conditions (pH 7.4, 37 °C) (Fig. 2A). Other combinations, such as the mixture of unmodified HA/GEL or the modification of either component alone (HA/GEL-Ga or HA-Ga/GEL) did not form hydrogels (G′ < G″). The G′ value of the gallol ECM hydrogels (1 Hz) was 121.9 ± 7.8 Pa, whereas other groups were less than 5 Pa (Fig. 2B). The rapid gelation results from the gallol groups in both polymers being involved in non-covalent, reversible crosslinking of gallol-to-GEL (e.g., protein backbone) or gallol-to-gallol [38,39]. Gelation occurred in the gallol ECM at mass ratios of 1:1 and 1:2, but not with HA-Ga alone (e.g., 2wt%) (Fig. 2C), and the 1:2 formulation exhibited G′ values ~20 times higher than that of HA-Ga alone (Fig. 2D). We also tested gelation of the gallol ECM at a low concentration of HA-Ga (e.g., 1.6wt%), which resulted in mechanically weak hydrogels with a G′ value of 50.2 Pa (1 Hz) (Fig. S2).

Similar to our previous results [38], the gallol ECM hydrogel exhibited shear-thinning behavior due to dynamic hydrogen bonds among the gallol moieties and intermolecular interactions between gallol and gelatin backbones (Fig. 2E). This is illustrated through a general decrease in viscosity with increasing shear rate (0.05-100 $s^{-1}$) [45]. Hydrogels with a mass ratio of 1:1 exhibited similar shear-thinning behavior at shear rates higher than 0.05 $s^{-1}$, yet the viscosity at shear rates lower than 0.05 $s^{-1}$ decreased from ~850 Pa·s for that of 1:2 hydrogels to ~250 Pa·s, potentially due to a decrease in crosslinking density [46]. The shear-thinning behavior of these gels is also qualitatively displayed via extrusion of the gallol ECM hydrogels through a narrow 25 gauge needle (inner diameter = 0.26 mm) (Fig. 2F).

### 3.2. Temporal self-healing behavior of the gallol ECM hydrogels

In addition to immediate association with proteins via non-covalent hydrogen bonds [38,39], gallol groups will undergo auto-oxidation to hydroquinone with covalent crosslinking over several hours (~120 min) [47]. Thus, we expected that the dominant driving forces involved in gelation would temporally exchange, that is, from dynamic, non-covalent bonds for short times (e.g., 10 s to min) to covalent crosslinking for longer times (e.g., hrs to days). For comparison, we prepared gallol ECM hydrogels with a mass ratio of 1:2 and analyzed them immediately or after aging for one day at room temperature. As expected, the G′ and G″ values of the aged hydrogels were higher than those of the hydrogels tested immediately after gelation (Fig. 3A). Specifically, the G′ value (1 Hz) of the aged hydrogels was ~2.8 times higher than that of the immediately formed hydrogels (Fig. 3B) and the Young's

modulus increased from $1.5 \pm 0.3$ kPa to $2.3 \pm 0.2$ kPa with aging (Fig. 3C). There were minimal further changes in the hydrogel after 24 h aging (results not shown). These results indicate that the newly generated covalent bonds by auto-oxidation of gallols enhance the hydrogel crosslinking density, resulting in increased mechanical properties.

Beyond the mechanics, we assessed the self-healing properties of the gallol ECM hydrogels formed immediately (Day 0) or after one day of aging. For hydrogels tested within 30 min of gelation, rapid adhesion was apparent when pieces of hydrogel were placed together for 15 min due to hydrogen bonding between pieces. However, after aging for one day, there was little adhesion between pieces during 15 min of incubation, likely since the gallol groups had undergone covalent bonding and were no longer available for interactions across the hydrogel pieces (Fig. 3D). The shear-thinning and recovery of gallol ECM hydrogels was also quantitatively measured under alternating oscillatory strain at a fixed frequency of 1 Hz for hydrogels formed immediately (Fig. 3E) or after one day of aging (Fig. 3F). For hydrogels tested immediately after gelation, rapid shear-thinning was observed when the shear was increased (from 0.5 to 1000%) and the hydrogels partially recovered up to ~55% when the strain was decreased (from 1000 to 0.5%). After 10 min, the $G'$ recovered back to ~80% of the original value. In contrast, although the aged hydrogels exhibited shear-thinning when the shear was increased (from 0.5 to 2000%), there was a limited recovery of only 11% when the strain was decreased (from 1000 to 0.5%). This is likely due to the fracture of covalent bonds during shear-thinning of aged hydrogels without a mechanism for rapid recovery. Although initially formed hydrogels present a certain degree of covalent bonds, dynamic, reversible bonds are still dominant in the gelation and recovery processes.

### 3.3. The physicochemical mechanism of the gallol ECM gelation

To better understand our proposed mechanism of temporal crosslinking – where immediate gelation largely results from dynamic, hydrogen bonds and further aging of gallol ECM hydrogels introduces further covalent crosslinking – we conducted a number of additional rheological and spectroscopic studies where crosslinking was perturbed. First, rheological experiments were performed using various solvents, including PBS, deionized water (DDW), and excessive treatment of urea (Fig. 4A). A change in the solvent (PBS versus DDW) alters the oxidation of gallols (e.g., formation of covalent bonds), meaning that only hydrogen bonds exist in early gelation with DDW; treatment with urea inhibits the formation of hydrogen bonds, meaning that only oxidative crosslinking is present. In particular, urea is known to disrupt hydrogen bonds in polysaccharides [48]. As expected, with DDW as a solvent (e.g., no buffering to neutral pH), gelation occurred ($G' > G''$), but with $G'$ (1 Hz) decreasing to 34.4 Pa from the control of PBS at 135.8 Pa. Urea treatment (1 M) still permitted gelation, but also with a decreased $G'$ (1 Hz) of 32.6 Pa. Taken together, these results demonstrate that the gallol hydrogels prepared in PBS include both hydrogen bonds and some covalent bonds directly after mixing, which can be blocked using urea treatment or DDW, respectively.

ATR-IR spectroscopy was performed for solutions of HA-Ga and GEL-Ga, as well as the gallol ECM hydrogel of HA-Ga/GEL-Ga to better understand hydrogen bonding within the hydrogel system (Fig. 4B). Notable shifts appeared at the O—H stretching vibrational bands

and the strongest amide I peak obtained from HA and GEL backbones occurred when they were mixed. The O—H stretching vibration was centered at 3332 cm$^{-1}$ for HA-Ga alone and 3308 cm$^{-1}$ for GEL-Ga alone. However, in the mixture of HA-Ga/GEL-Ga, the O—H band was dramatically shifted down to 3293 cm$^{-1}$. Furthermore, the amide I peak (C=O stretch) was detected at 1607 cm$^{-1}$ for HA-Ga alone, 1644 cm$^{-1}$ for GEL-Ga alone, and 1632 cm$^{-1}$ for HA-Ga/GEL-Ga mixtures. The C=O peak shift of the mixture to a lower wavenumber might be attributed to hydrogen bonds between gallol and protein backbones, similar to previously observed spectral shifts in peptide/protein hydrogels arrayed by hydrogen bonds [49].

UV/vis spectral analysis was also used to investigate auto-oxidation of gallol polymers as a function of time (Figs. S3 and 4). The intrinsic absorption peak of the gallol dimers generated by auto-oxidation (e.g., gallol → hydroquinone) at 420–440 nm [47] was monitored for HA-Ga, GEL-Ga (Fig. S3) and the HA-Ga/GEL-Ga mixture dissolved in PBS or DDW (Fig. 4C). Considering the background absorption level of PBS alone ($A_{420} =$ 0.028), the absorbance of GEL-Ga dissolved in DDW was 0.046, indicating that within 15 min GEL-Ga undergoes some degree of auto-oxidation (Fig. S3); during the synthesis of GEL-Ga (e.g., at high temperatures of 40–50 °C), there is a slight increase in oxygen radical formation such that auto-oxidation is induced [50]. The absorbance of the HA-Ga/GEL-Ga noticeably increased when PBS was used as a solvent rather than DDW, owing to enhanced auto-oxidation of gallols at neutral pH (Fig. 4C). The overall schematic for the mechanism of crosslinking with gallol chemistry is shown in Fig. 4D, where the gallol ECM polymers (HA-Ga, GEL-Ga) interact via hydrogen bonds mainly with amide polymeric backbones for initial gelation (left) and are subsequently aged via auto-oxidation (right), leading to increased mechanical properties.

### 3.4. 3D printing using the gallol ECM hydrogels and cytocompatibility

Utilizing the unique properties of the gallol groups, temporal shear-thinning and oxidative crosslinking, extrusion-based 3D printing was performed (Fig. 5A), including with encapsulated fibroblasts for culture up to 6 days (Fig. 6A). Fibroblasts are the most common cells in almost all connective tissues and were used here as a model cell for viability analysis. As expected, based on the crosslinking mechanism, shape fidelity of the printed filaments was dependent on gallol ECM hydrogel concentration and time from mixing (Fig. 5B). Specifically, for good printability, the gallol ECM hydrogel ink was printed at a mass ratio of 1:2 (e.g., HA-Ga: GEL-Ga), a total concentration of 6 wt% and within 0.5 h of mixing, leading to stable filaments initially and after incubation in PBS with 10% BSA (Fig. 5C). Other ink formulations exhibited moduli that were not high enough at low concentrations or too much covalent crosslinking at long times, both leading to discontinuous filaments. Heterogeneity in printed filaments was further observed during the extrusion and formation of lattice structures via the inclusion of fluorophores within filaments (Fig. 5D). However, when printing was performed within 0.5 h after mixing HA-Ga and GEL-Ga, uniform flow of the gallol ink was maintained during extrusion, and the obtained lattice structure showed clear square shapes at the crossing of filaments. In contrast, filament flow while printing became slightly inconsistent at 1 h after mixing HA-Ga and GEL-Ga, and the heterogeneity of filaments further increased at 2 h.

In addition to basic printability, printing shortly after mixing also showed improved cell viability when compared to longer times after mixing, potentially due to reduced shear forces on cells with lower crosslinking (Fig. 6B and C). When a cell-laden ink was printed within 0.5 h of mixing gel components, cell viability was high at $95.9 \pm 1.9\%$ and not statistically significant when compared to non-printed cells at $96.8 \pm 0.6\%$. However, when printing was performed 1 or 2 h after mixing gel components, cell viability decreased to $78.6 \pm 8.9\%$ and $80.1 \pm 4.2\%$, respectively. Thus, for subsequent experiments involving long-term cell culture in printed constructs, printing was performed within 0.5 h of ink preparation (e.g., Day 0 in Fig. 6E-G).

To better understand the performance of printed filaments in culture, hydrogel degradation, cell viability and spreading were monitored. After gelation, gallol ECM hydrogels initially swelled for 2 days and thereafter gradually degraded over 14 days (Fig. S4). This swelling and degradation increased the width of printed filaments over time ($1100.7 \pm 92$ μm for Day 1 to $2895.2 \pm 178$ μm for Day 6) (Fig. S5A). Cell viability decreased with 1 day of aging to $73.6 \pm 4.8\%$, but then increased to $92.5 \pm 1.9\%$ with further culture (Fig. 6D and E). In particular, the density of live cells increased by 1.5 times over six days of culture when compared to that of 'Day 1', likely indicating proliferation in the printed filaments (Fig. S5B). Additionally, cells transitioned from a rounded to spread morphology, likely due to the presence of adhesion and degradation sites in the filaments due to gelatin (Fig. 6F and G), whereas cells in HA hydrogels alone typically remained rounded [51]. Single cells with stained nuclei and F-actin also showed spreading at Day 6, which was distinct from the rounded morphology at Day 0 (Fig. 6F). Specifically, cell spread area increased from $102.0 \pm 19.7$ μm$^2$ initially to $374.0 \pm 104.9$ μm$^2$ at 6 days. Taken together, the gallol ECM hydrogel ink was successfully 3D printed with high cell viability and activity.

### 3.5. On-tissue printability and tissue adhesiveness of the gallol ECM hydrogel ink

One of the advantages of gallol modification includes tissue adhesiveness [36,37,40]. Thus, we expected that the gallol ECM hydrogel ink could be printable on tissue and that printed constructs would show adhesion to the tissue. Lung and heart tissues were chosen as model tissues to demonstrate the adhesion of the hydrogel inks for localization of printed constructs on tissues. Gallol ECM hydrogel inks were printed onto lung and heart tissues as examples (Fig. 7A). Owing to the adhesion of gallol filaments to tissue substrates, aligned filaments in one layer (top) or lattice structures consisting of two layers (bottom) were printed on each tissue and were stable to agitation. To better understand the adhesive strength of the gallol ECM hydrogel ink, printed hydrogels were used to adhere PDMS substrates (with dimensions of 1cm × 5 cm and thicknesses of 0.5 cm) together, which were then subjected to uniaxial tension (Fig. 7B and C). Testing was performed until failure and adhesive strengths were determined, clearly illustrating enhanced adhesive strengths for gallol-containing hydrogels ($18.7 \pm 2.4$ kPa) and lower adhesive strengths for non-gallol-containing mixtures ($12.3 \pm 0.4$ kPa) and PBS alone ($10.7 \pm 2.5$ kPa, due to self-adhesion of PDMS itself). In addition, the tissue adhesive strengths of 3D printed gallol hydrogels were evaluated against tensile stress applied to myocardial tissues (Fig. 7D and E). Similar to the results of PDMS substrates, printed gallol ECM hydrogels showed an increase in tissue adhesiveness ($1.4 \pm 0.3$ kPa) over non-gallol mixtures ($0.8 \pm 0.1$ kPa) and self-adhesion of the myocardium

tissue alone (0.7 ± 0.1 kPa). These results indicate gallol-derived adhesion properties, potentially achieving the enhanced localization of printed constructs onto tissues.

## 4. Discussion

There are numerous challenges to the development of biomaterial inks and those containing cells (e.g., bioinks) due to the requisite properties for extrusion-based printing and cytocompatibility of both the material and printing process. To address this, we designed and implemented a hydrogel system based on gallol modification of ECM components, particularly HA and GEL. This hydrogel exhibits temporal crosslinking, with shear-thinning properties early due to largely dynamic hydrogen bonding that dominates over covalent crosslinking, and stabilization over time due to non-dynamic oxidative processes. This process was well characterized through rheological characterization and fundamental spectroscopy studies, and 3D printing was conducted both without and with encapsulated cells.

To the best of our knowledge, only a few studies on gallol-modified polymers have focused on wet-resistant adhesiveness [36,37]. However, gallol-containing molecules are known for a strong binding affinity to proline-rich proteins via hydrogen bonds, resulting in astringent taste when interacting with salivary tissues [35]. Gelatin is also proline-rich [52], allowing us to hypothesize that gallol-modified polymers would crosslink with gelatin to form hydrogels. However, the intermolecular interaction of gallol-modified HA with gelatin alone could not form hydrogels (Fig. 2A), likely due to insufficient hydrogen bonding. Thus, the gallol modification was performed on both HA and gelatin, and as previously reported [38], immediate gelation occurred because of multiple non-covalent interactions between the polymers. In addition to non-covalent interactions of gallols, use of neutral buffer (PBS, pH 7.4) enhanced auto-oxidation of gallols followed by gradual covalent crosslinking. As the ECM is a complex mixture of polysaccharides (HA and heparin sulfate) and proteins (collagen, fibronectin and laminin) physically entangled by hydrogen bonds [53], this approach can be used to mimic many characteristics of the ECM.

Towards bioprinting applications, the gallol ECM hydrogel ink could be incorporated into the printing process by simply mixing the two components. This gelation mechanism avoids the use of other additives for viscosity modulation or the use of photocrosslinking chemistry and introduction of radicals for stabilization of the printed structure. As cells are sensitive to their surroundings and processing steps, it is important to ensure that the conditions for gelation are mild. We found that bioprinted cell-laden gallol hydrogels exhibited high cell viability of ~95% and supported cell proliferation and spreading due to the incorporation of degradable ECM components. The gallol modification (~10–15%) enabled gelation using a low concentration of gelatin (both 2 and 4wt%), which is distinct from the high concentration (7–15wt%) for gelation of traditional gelatin-based bioinks. Considering the sensitivity of cells to the mechanical stiffness of materials [54], the gallol ECM bioinks could be tailored for a wide range of soft tissue applications.

Finally, gallol ECM hydrogel inks showed printability on tissue and the existence of gallols within the ink enhanced the tissue adhesiveness of printed structures. The ultimate goal of

these 3D fabricated scaffolds is to be implanted *in vivo* for the repair and regeneration of tissues [55], and implanted scaffolds should be located in desirable positions corresponding to damaged tissues. Thus, an increase in tissue adhesion through the use of gallol-modified bioinks would improve final localization of those structures in *in vivo* environments. ECM-mimetic adhesive constructs using unique gallol formulations would suggest widespread applications for tissue repair, implant localization, and 3D modeling for pharmaceutical screening.

## 5. Conclusions

We have developed gallol-modified ECM hydrogel inks exhibiting early shear-thinning behavior, spontaneous covalent crosslinking, and tissue adhesion for 3D bioprinting. Hydrogels formed rapidly with simple mixing of gallol-modified HA and GEL at low concentrations (e.g., 6 wt%) by dynamic, non-covalent hydrogen bonds, which allowed extrusion for 3D printing. The hydrogel constructs then aged with enhanced mechanical properties by gradual oxidative crosslinking of gallol moieties without any external stimuli. When used as a cell-laden gallol-modified hydrogel ink, ~95% of loaded cells were alive after the 3D printing process, and both proliferation and spreading of cells were observed in printed constructs. The hydrogel ink was also printable onto tissue substrates, such as heart and lung, owing to the unique property of the adhesion of gallol groups to ECM, which could aid in implantation and localization of printed constructs. Thus, our finding for a new type of gallol hydrogel ink inspired by rapid fruit browning phenomena is a promising approach to fabricate a variety of 3D printed constructs targeting soft tissue repair.

## Supplementary Material

Refer to Web version on PubMed Central for supplementary material.

## Acknowledgements

## References

[1]. Williams D, Thayer P, Martinez H, Gatenholm E, Khademhosseini A, A perspective on the physical, mechanical and biological specifications of bioinks and the development of functional tissues in 3D bioprinting, Bioprinting 9 (2018) 19–36.

[2]. You F, Eames BF, Chen X, Application of extrusion-based hydrogel bioprinting for cartilage tissue engineering, Int. J. Mol. Sci 18 (2017) 1597.

[3]. Hölzl K, Lin S, Tytgat L, Van Vlierberghe S, Gu L, Ovsianikov A, Bioink properties before, during and after 3D bioprinting, Biofabrication 8 (2016) 032002. [PubMed: 27658612]

[4]. Chang R, Emami K, Wu H, Sun W, Biofabrication of a three-dimensional liver micro-organ as an in vitro drug metabolism model, Biofabrication 2 (2010) 045004. [PubMed: 21079286]

[5]. Vanderburgh J, Sterling JA, Guelcher SA, 3D printing of tissue engineered constructs for in vitro modeling of disease progression and drug screening, Ann. Biomed. Eng 45 (2017) 164–179. [PubMed: 27169894]

[6]. Norman J, Madurawe RD, Moore CMV, Khan MA, Khairuzzaman A, A new chapter in pharmaceutical manufacturing: 3D-printed drug products, Adv. Drug Deliv. Rev 108 (2017) 39–50. [PubMed: 27001902]

[7]. Lepowsky E, Tasoglu S, 3D printing for drug manufacturing: a perspective on the future of pharmaceuticals, Int. J. Bioprint 4 (2018) 1.

[8]. Song KH, Highley CB, Rouff A, Burdick JA, Complex 3D-printed microchannels within cell-degradable hydrogels, Adv. Funct. Mater 1801331 (2018).

[9]. Brandenberg N, Lutolf MP, In situ patterning of microfluidic networks in 3D cell-laden hydrogels, Adv. Mater 28 (2016) 7450–7456. [PubMed: 27334545]

[10]. Selimis A, Mironov V, Farsari M, Direct laser writing: principles and materials for scaffold 3D printing, Microelectron. Eng 132 (2015) 83–89.

[11]. Moroni L, Schotel R, Hamann D, de Wijn JR, van Blitterswijk CA, 3D fiber-deposited electrospun integrated scaffolds enhance cartilage tissue formation, Adv. Funct. Mater 18 (2008) 53–60.

[12]. Jin G, Shin M, Kim S-H, Lee H, Jang J-H, SpONGE: spontaneous organization of numerous-layer generation by electrospray, Angew. Chem. Int. Ed 54 (2015) 7587–7591.

[13]. Kolesky DB, Truby RL, Gladman AS, Busbee TA, Homan KA, Lewis JA, 3D bioprinting of vascularized, heterogeneous cell-laden tissue constructs, Adv. Mater 26 (2014) 3124–3130. [PubMed: 24550124]

[14]. Bertassoni LE, Cardoso JC, Manoharan V, Cristino AL, Bhise NS, Araujo WA, Zorlutuna P, Vrana NE, Ghaemmaghami AM, Dokmeci MR, Khademhosseini A, Direct-write bioprinting of cell-laden methacrylated gelatin hydrogels, Biofabrication 6 (2014) 024105. [PubMed: 24695367]

[15]. Ozbolat IT, Hospodiuk M, Current advances and future perspectives in extrusion-based bioprinting, Biomaterials 76 (2016) 321–343. [PubMed: 26561931]

[16]. Tibbitt MW, Anseth KS, Hydrogels as extracellular matrix mimics for 3D cell culture, Biotechnol. Bioeng 103 (2009) 655–663. [PubMed: 19472329]

[17]. Ouyang L, Highley CB, Rodell CB, Sun W, Burdick JA, 3D printing of shear-thinning hyaluronic acid hydrogels with secondary cross-linking, ACS Biomater. Sci. Eng 2 (2016) 1743–1751. [PubMed: 33440472]

[18]. Hong S, Sycks D, Chan HF, Lin S, Lopez GP, Guilak F, Leong KW, Zhao X, 3D printing of highly stretchable and tough hydrogels into complex, cellularized structures, Adv. Mater 27 (2015) 4035–4040. [PubMed: 26033288]

[19]. Lee D, Park JP, Koh M-Y, Kim P, Lee J, Shin M, Lee H, Chitosan-catechol: a writable bioink under serum culture media, Biomater. Sci 6 (2018) 1040–1047. [PubMed: 29666857]

[20]. Ng WL, Goh MH, Yeong WY, Naing MW, Applying macromolecular crowding to 3D bioprinting: fabrication of 3D hierarchical porous collagen-based hydrogel constructs, Biomater. Sci 6 (2018) 562–574. [PubMed: 29383354]

[21]. Yeo MG, Kim GH, A cell-printing approach for obtaining hASC-laden scaffolds by using a collagen/polyphenol bioink, Biofabrication 9 (2017) 025004. [PubMed: 28402968]

[22]. Pati F, Jang J, Ha DH, Kim SW, Rhie JW, Shim JH, Kim D-H, Cho D-W, Printing three-dimensional tissue analogues with decellularized extracellular matrix bioink, Nat. Commun 5 (2014) 3935. [PubMed: 24887553]

[23]. Yue K, Santiago GT, Alvarez MM, Tamayol A, Annabi N, Khademhosseini A, Synthesis, properties, and biomedical applications of gelatin methacryloyl (GelMA) hydrogels, Biomaterials 73 (2015) 254–271. [PubMed: 26414409]

[24]. Rutz AL, Hyland KE, Jakus AE, Burghardt WR, Shah RN, A multimaterial bioink method for 3D printing tunable, cell-compatible hydrogels, Adv. Mater 27 (2015) 1607–1614. [PubMed: 25641220]

[25]. Kang H-W, Lee SJ, Ko IK, Kengla C, Yoo JJ, Atala A, A 3D bioprinting system to produce human-scale tissue constructs with structural integrity, Nat. Biotechnol 34 (2016) 312–319. [PubMed: 26878319]

[26]. Xu T, Binder KW, Albanna MZ, Dice D, Zhao W, Yoo JJ, Atala A, Hybrid printing of mechanically and biologically improved constructs for cartilage tissue engineering applications, Biofabrication 5 (2013) 015001. [PubMed: 23172542]

[27]. Li H, Liu S, Li L, Rheological study on 3D printability of alginate hydrogel and effect of graphene oxide, Int. J. Bioprint 2 (2016) 54–66.

[28]. Tan EYS, Yeong WY, Concentric bioprinting of alginate-based tubular constructs using multi-nozzle extrusion-based technique, Int. J. Bioprint 1 (2015)49–56.

[29]. Hong SH, Shin M, Lee J, Ryu JH, Lee S, Yang JW, Kim WD, Lee H, STAPLE: stable alginate gel prepared by linkage exchange from ionic to covalent bonds, Adv. Healthcare Mater 5 (2016) 75–79.

[30]. Highley CB, Rodell CB, Burdick JA, Direct 3D printing of shear-thinning hydrogels into self-healing hydrogels, Adv. Mater 27 (2015) 5075–5079. [PubMed: 26177925]

[31]. Wang LL, Highley CB, Yeh Y-C, Galarraga JH, Uman S, Burdick JA, Three-dimensional extrusion bioprinting of single- and double-network hydrogels containing dynamic covalent crosslinks, J. Biomed. Mater. Res. Part A 106A (2018) 865–875.

[32]. Quideau S, Deffieux D, Douat-Casassus C, Pouységu L, Plant polyphenols: chemical properties, biological activities, and synthesis, Angew. Chem. Int. Ed 50(2011) 586–621.

[33]. Yokotsuka K, Shimizu T, Shimizu T, Polyphenoloxidase from six mature grape varieties and their activities towards various phenols, J. Ferment. Bioeng 71 (1991) 156–162.

[34]. Tanaka T, Takahashi R, Kouno I, Nonaka G, Chemical evidence for the deastringency (insolubilization of tannins) of persimmon fruit, J. Chem. Soc. Perkin Trans 1 (1994) 3013–3022.

[35]. Luck G, Liao H, Murray NJ, Grimmer HR, Warminski EE, Williamson MP, Lilley TH, Haslam E, Polyphenols, astringency and proline-rich proteins, Phytochemistry 37 (1994) 357–371. [PubMed: 7765619]

[36]. Zhan K, Kim C, Sung K, Ejima H, Yoshie N, Tunicate-inspired gallol polymers for underwater adhesive: a comparative study of catechol and gallol, Biomacromolecules 18 (2017) 2959–2966. [PubMed: 28853566]

[37]. Cho JH, Lee JS, Shin J, Jeon EJ, An S, Choi YS, Cho S-W, Ascidian-inspired fast-forming hydrogel system for versatile biomedical applications: pyrogallol chemistry for dual modes of crosslinking mechanism, Adv. Funct. Mater 28 (2018) 1705244.

[38]. Shin M, Lee H, Gallol-rich hyaluronic acid hydrogels: Shear-thinning, protein accumulation against concentration gradients, and degradation-resistant properties, Chem. Mater 29 (2017) 8211–8220.

[39]. Shin M, Lee H-A, Lee M, Shin Y, Song J-J, Kang S-W, Nam D-H, Jeon EJ, Cho M, Do M, Park SH, Lee MS, Jang J-H, Cho S-W, Kim K-S, Lee H, Targeting protein and peptide therapeutics to the heart via tannic acid modification, Nat. Biomed. Eng 2 (2018) 304–317. [PubMed: 30936449]

[40]. Shin M, Ryu JH, Park JP, Kim K, Yang JW, Lee H, DNA/tannic acid hybrid gel exhibiting biodegradability, extensibility, tissue adhesiveness, and hemostatic ability, Adv. Funct. Mater 25 (2015) 1270–1278.

[41]. Weisburg JH, Weissman DB, Sedaghat T, Babich H, In vitro cytotoxicity of epigallocatechin gallate and tea extracts to cancerous and normal cells from the human oral cavity, Basic Clin. Pharmacol 95 (2004) 191–200.

[42]. Ainsworth EA, Gillespie KM, Estimation of total phenolic content and other oxidation substrates in plant tissues using Folin-Ciocalteu reagent, Nat. Protoc 2 (2007) 875–877. [PubMed: 17446889]

[43]. Claaßen C, Claaßen MH, Truffault V, Sewald L, Tovar GEM, Borchers K, Southan A, Quantification of substitution of gelatin methacryloyl: best practice and current pitfalls, Biomacromolecules 19 (2018) 42–52. [PubMed: 29211461]

[44]. Zhou L, Tan G, Tan Y, Wang H, Liao J, Ning C, Biomimetic mineralization of anionic gelatin hydrogels: effect of degree of methacrylation, RSC Adv. 4 (2014) 21997–22008.

[45]. Guvendiren M, Lu HD, Burdick JA, Shear-thinning hydrogels for biomedical applications, Soft Matter 8 (2012) 260–272.

[46]. Xu D, Liu C-Y, Craig SL, Divergent shear thinning and shear thickening behavior of supramolecular polymer networks in semidilute entangled polymer solutions, Macromolecules 44 (2011) 2343–2353. [PubMed: 21547008]

[47]. Abrash HI, Shih D, Elias W, Malekmehr F, A kinetic study of the air oxidation of pyrogallol and purpurogallin, Int. J. Chem. Kinet 21 (1989) 465–476.

[48]. Mcqueen-Mason S, Cosgrove DJ, Disruption of hydrogen bonding between plant cell wall polymers by proteins that induce wall extension, Proc. Natl. Acad. Sci. U.S.A 91 (1994) 6574–6578. [PubMed: 11607483]

[49]. Kiyonaka S, Sada K, Yoshimura I, Shinkai S, Kato N, Hamachi I, Semi-wet peptide/protein array using supramolecular hydrogel, Nat. Mater 3 (2004) 58–64. [PubMed: 14661016]

[50]. De AK, Chaudhuri B, Bhattacharjee S, A kinetic study of the oxidation of phenol, o-chlorophenol and catechol by hydrogen peroxide between 298 K and 333 K: the effect of pH, temperature and ratio of oxidant to substrate, J. Chem. Technol. Biotechnol 74 (1999) 162–168.

[51]. Ouyang L, Highley CB, Sun W, Burdick JA, A generalizable strategy for the 3D bioprinting of hydrogels from nonviscous photo-crosslinkable inks, Adv. Mater 29 (2017) 1604983.

[52]. Eastoe JE, The amino acid composition of mammalian collagen and gelatin, Biochem. J 61 (1955) 589–600. [PubMed: 13276342]

[53]. Mouw JK, Ou G, Weaver VM, Extracellular matrix assembly: a multiscale deconstruction, Nat. Rev. Mol. Cell Biol 15 (2014) 771–785. [PubMed: 25370693]

[54]. Discher DE, Janmey P, Wang Y-L, Tissue cells feel and respond to the stiffness of their substrate, Science 310 (2005) 1139–1143. [PubMed: 16293750]

[55]. Do A-V, Khorsand B, Geary SM, Salem AK, 3D printing of scaffolds for tissue regeneration applications, Adv. Healthcare Mater 4 (2015) 1742–1762.
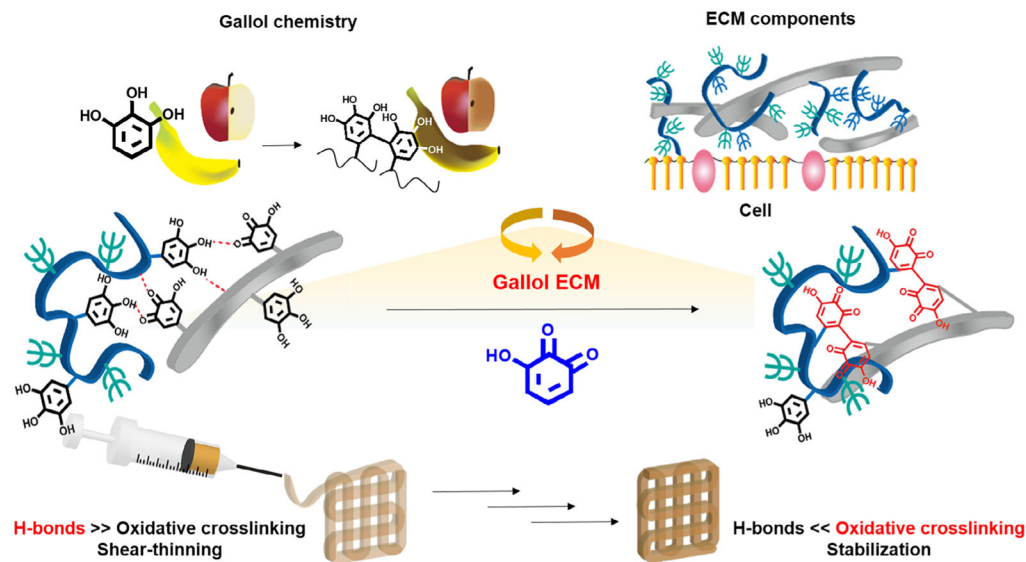
**Fig. 1.**

Schematic description of the formation and extrusion of gallol ECM hydrogels, with crosslinking inspired by rapid fruit browning chemistry. On short time-scales, the hydrogels are formed by dynamic hydrogen bonds that permit shear-thinning behavior, whereas on longer time-scales the auto-oxidation of gallol groups leads to stabilization by covalent bonds.
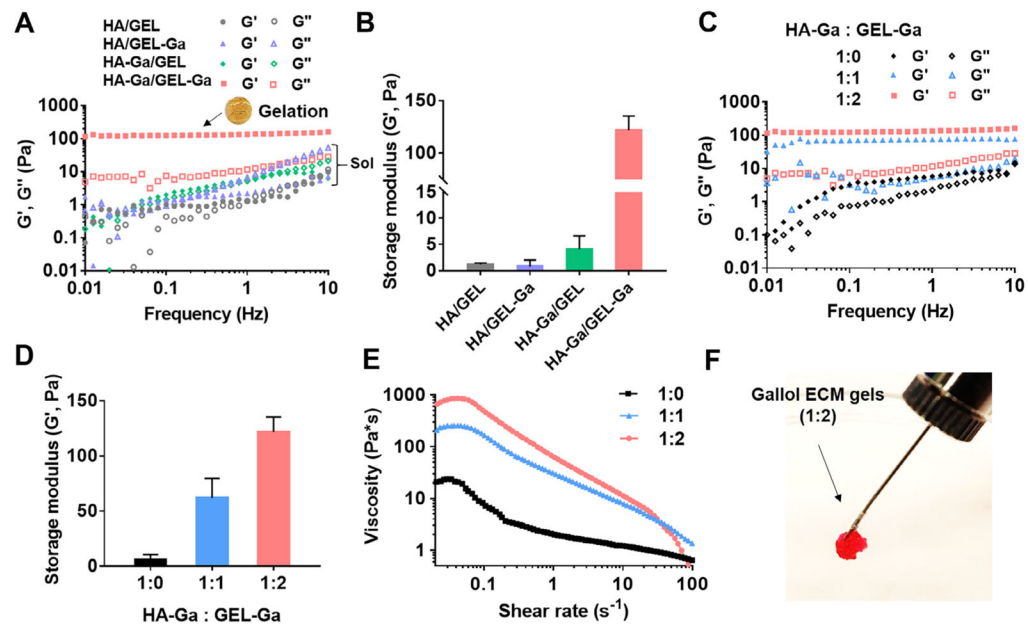
**Fig. 2.**

Mechanical characterization and extrusion of gallol ECM hydrogels immediately after mixing. (A) Frequency sweep (storage ($G'$) and loss ($G''$) moduli at 0.5% strain, 37 °C) and (B) $G'$ (1 Hz) of mixtures of non-gallol (hyaluronic acid (HA), gelatin (GEL)) and gallol (HA-Ga, GEL-Ga) polymers at 1:2 mass ratio and total concentration of 6 wt%. Gelation occurred only with the mixture of HA-Ga and GEL-Ga (inset photo of formed hydrogel). (C) Frequency sweep, (D) $G'$ (1 Hz), and (E) viscosity with increasing shear rate of the gallol ECM hydrogels with various HA-Ga:GEL-Ga mass ratios. (F) Macroscopic injectability of the rhodamine-containing gallol hydrogel (HA-Ga:GEL-Ga of 1:2) with a 25 G needle.
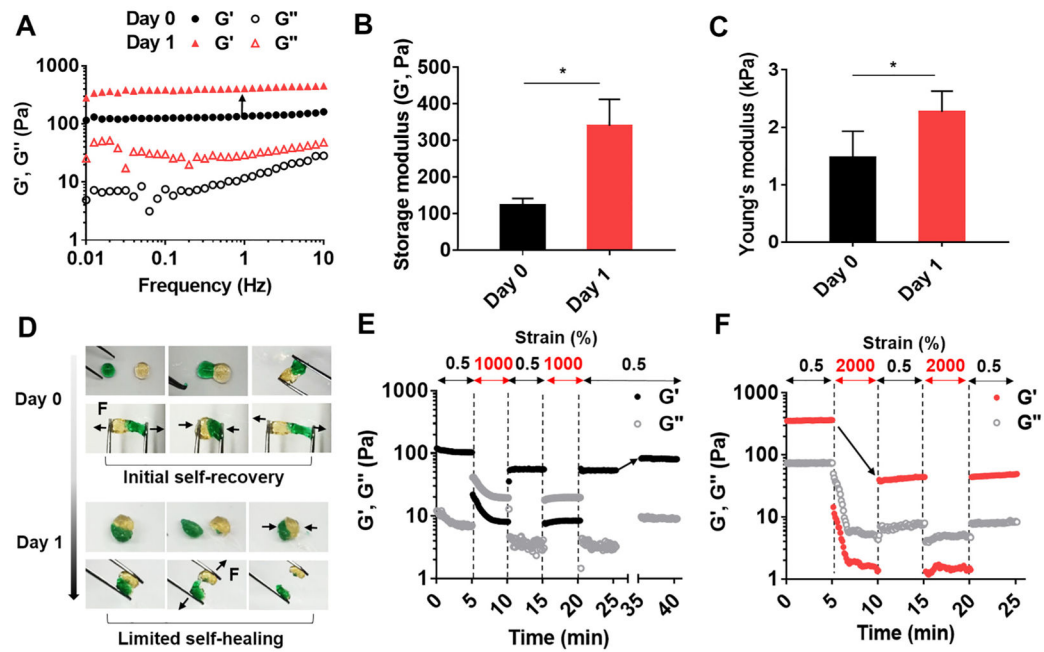
**Fig. 3.**
Changes in mechanical properties and self-healing of the gallol ECM hydrogels with aging. (A) Frequency sweep (storage (G′) and loss (G″) moduli at 0.5% strain, 37 °C), (B) G′ (1 Hz), and (C) Young's moduli of gallol (HA-Ga, GEL-Ga) hydrogels at 1:2 mass ratio and 6 wt% initially (Day 0) and 1 day after gelation. (D) Macroscopic self-healing of hydrogels initially (Day 0) and limited self-healing 1 day after gelation. The black arrows indicate the direction of physical forces (F) applied to the hydrogels. Evaluation of disruption and recovery of hydrogels (E) initially (intermittent strains of 0.5 and 1000%) and (F) 1 day after gelation (intermittent strains of 0.5 and 2000%). The black arrow in (E) indicates ~ 80% recovery of G′. The black arrow in (F) indicates a dramatic decrease of G′, corresponding to ~11% of the original value with one round of increased strain. Unpaired $t$-test, *$p < 0.05$.
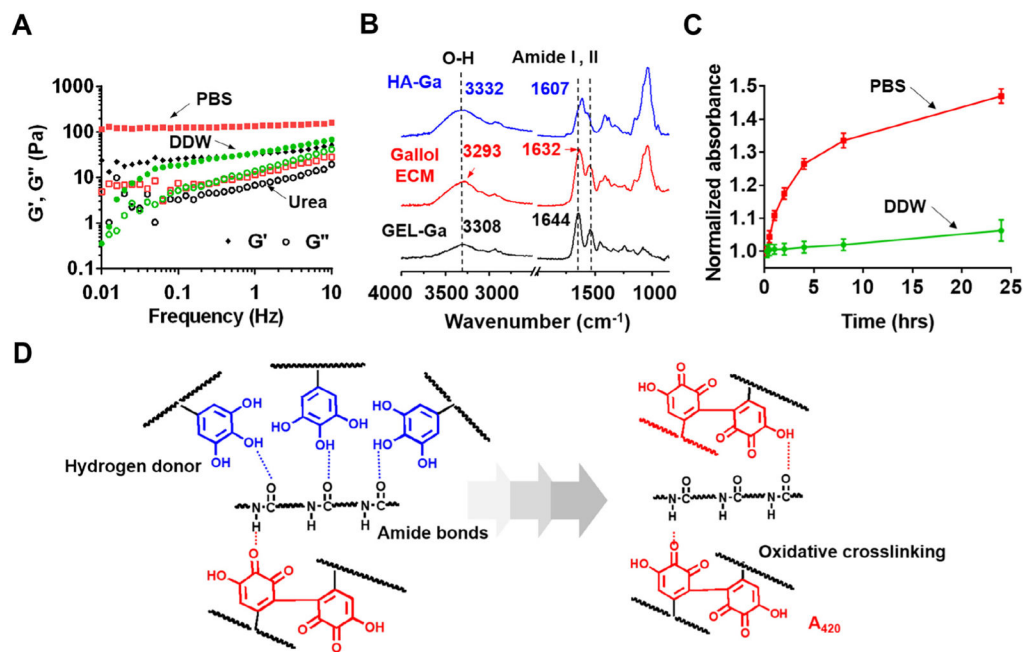
**Fig. 4.**

Physicochemical mechanism for the gallol ECM gelation. (A) Frequency sweep (storage (G ′) and loss (G″) moduli at 0.5% strain, 37 °C) of gallol (HA-Ga, GEL-Ga) hydrogels at 1:2 mass ratio and 6 wt% formed in phosphate buffered saline (PBS, red symbols) or with either deionized water (DDW, green symbols), or treatment of urea (1 M, black symbols). (B) ATR-IR spectra of the gallol ECM (red), HA-Ga alone (blue), and GEL-Ga alone (black). (C) Normalized (to values at 15 min) absorption (420 nm) of the gallol ECM mixtures prepared in PBS (red) or DDW (green) as a function of time. (D) Proposed gelation mechanism of temporally changing hydrogen bonds of the gallols with amide backbones (left panel, blue dashed line) to covalent crosslinking via gallol auto-oxidation (right panel, red compounds).
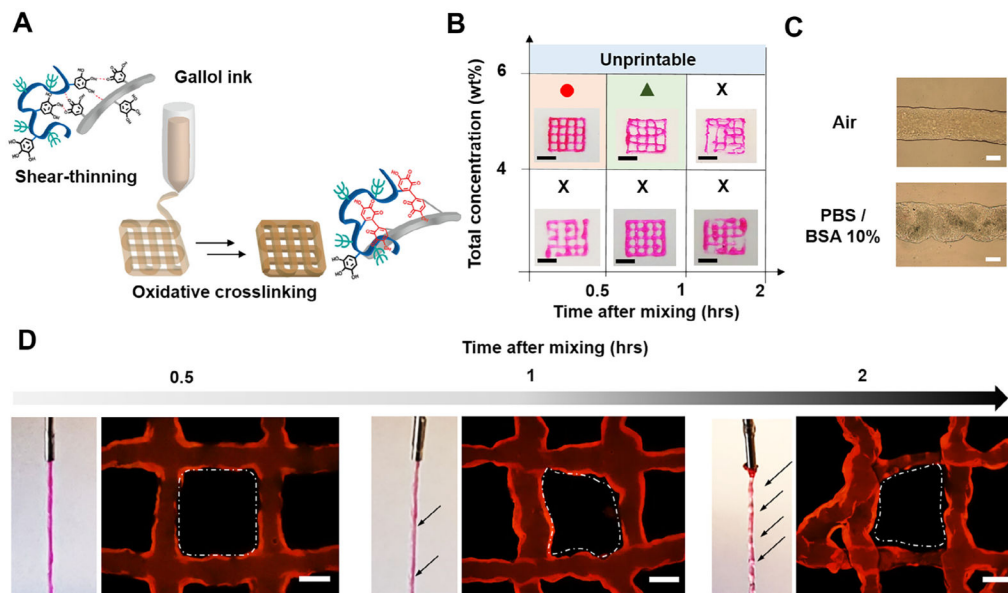
**Fig. 5.**

3D printing of gallol ECM hydrogel inks. (A) Schematic illustration of the 3D printing where the ink transitions from a shear-thinning hydrogel during printing to one with mechanical stabilization via oxidation after the printing. (B) Printability of the gallol ECM ink with various concentrations (4, 6 wt%) and injectability as a function of the time after gel formation (0.5, 1, 2 h). Scale bars of 4 mm. (C) Morphology of a printed filament using the gallol ECM ink (1:2 mass ratio, 6 wt%) immediately after printing in air (top) and after 30 min incubation in PBS with 10% BSA (bottom). (D) Representative images of printed filaments and printed lattice structures after 0.5,1, and 2 h. The black arrows show the irregular regions of the filaments and the white dashed lines indicate heterogeneous shapes within the lattices. Scale bars: 500 μm for C, D.
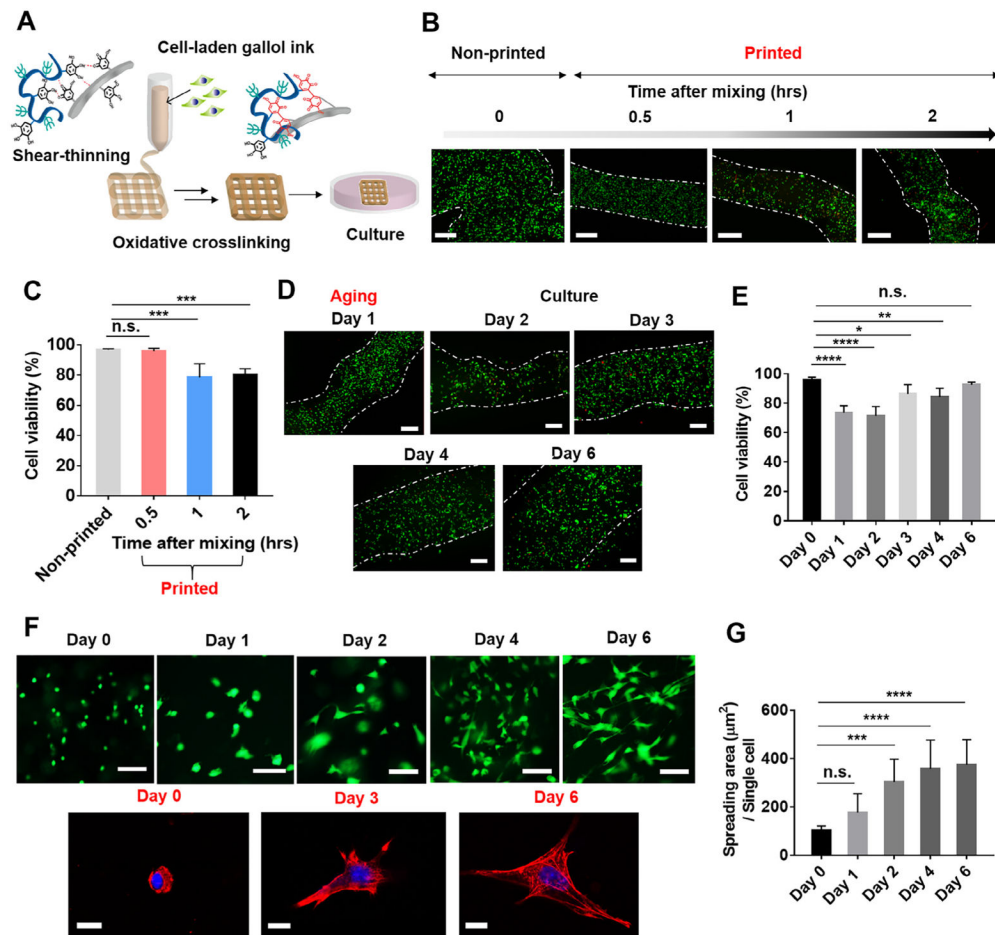
**Fig. 6.**
Cytocompatibility of cell-laden gallol ECM hydrogel inks. (A) Schematic description of the 3D printing of cell-laden gallol ECM inks and subsequent cell culture. (B) Fluorescent images and (C) quantification of live (green)/dead cells (red) in non-printed bulk hydrogels or printed filaments as a function of time after gel formation. (D) Fluorescent images and (E) quantification of live (green)/dead cells (red) in printed filaments after one-day of aging (Day 1) and during culture (Days 2-6). White dashed lines for (B) and (D) are approximate filament boundaries. (F) Fluorescent images of live/dead (top) and confocal images showing nuclei (blue) and F-actin (red) (bottom) of cells in printed constructs after encapsulation (Day 0) and during culture (Days 1-6). (G) Quantified spreading of the cells in printed filaments. Scale bars: 500 μm for B, D; 100 μm for top images of F; 10 μm for bottom images of F. Dunnett's test in conjunction with one-way ANOVA, n.s. (not significant), *p < 0.05, **p < 0.01, ***p < 0.001, ****p < 0.0001.
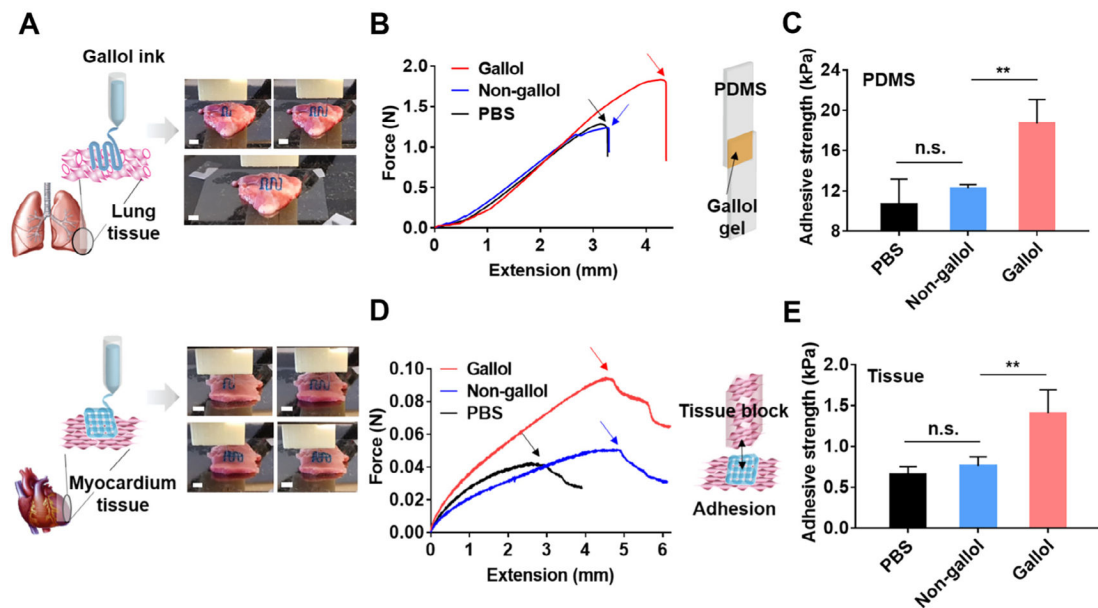
**Fig. 7.**
On-tissue 3D printing and adhesion of the gallol ECM hydrogel ink at 1:2 mass ratio and 6 wt%. (A) Schematics and images of printing of the gallol ink (containing blue food coloring dye) on porcine lung (top) and myocardium (bottom) tissues. Scale bars of 4 mm. (B) Force-extension curves and (C) quantification of adhesive strengths for the tensile testing of gallol hydrogels used to adhere PDMS substrates. The inset schematic shows the sample design and the arrows within the curves indicate the detachment of the materials from the PDMS substrates. (D) Force-extension curves and (E) quantification of adhesive strengths for the tensile testing of printed gallol ECM hydrogel lattices used to adhere myocardial tissues. The inset schematic corresponds to the experimental design for testing and the arrows within the curves indicate the detachment of the lattices from the myocardial substrates. Sidak test in conjunction with one-way ANOVA, n.s. (not significant) and **$p < 0.01$.